Directionally solidified fabrication in planar geometry of Al_2O_3-$Er_3Al_5O_{12}$ eutectic composite for thermophotovoltaic devices

D. Sola,[*] **P.B. Oliete, and J.I. Peña**

Instituto de Ciencia de Materiales de Aragón, Universidad de Zaragoza-CSIC, Departamento de Ciencia y Tecnología de Materiales y Fluidos, C/ María de Luna 3, 50.018 Zaragoza, Spain
[*]*dsola@unizar.es*

Abstract: In this work Al_2O_3–$Er_3Al_5O_{12}$ eutectic composite was manufactured in planar geometry departing from eutectic particles both produced by directional solidification using a CO_2 laser system at rates of 180 and 720 mm/h. Microstructure and mechanical properties were investigated as a function of the growth rate. Homogeneous and interpenetrated microstructure was found with phase size strongly dependent on the growth rate, decreasing when the processing rate was increased. Thermal emission of eutectic composites was studied in function of thermal excitation by using CO_2 laser radiation as a heating source. An intense narrow emission band at 1.55 µm matching with the sensitive region of the InGaAs photoconverter and a low emission band at 1 µm were obtained. Features of thermal emission bands were correlated with collecting angle, microstructure and laser power, and compared to those obtained from departing eutectic particles.

References and links

1. D. C. White, B. D. Wedlock, and J. Blair, "Recent advances in thermal energy conversion," in *Proc. 15th Ann. Power Sources Conf.* (1961), pp. 125–132.
2. G. E. Guazzoni, "High-temperature spectral emittance of oxides of erbium, samarium, neodymium and ytterbium," Appl. Spectrosc. **26**(1), 60–65 (1972).
3. C. R. Parent and R. E. Nelson, "Thermophotovoltaic energy conversion with a novel rare earth oxide emitter," in *Proc. 21st Intersoc. Energy Conv. Engg. Conf.* (1986), pp. 1314–1317.
4. D. L. Chubb, A. M. T. Pal, M. O. Patton, and P. P. Jenkins, "Rare earth doped high temperature ceramic selective emitters," J. Eur. Ceram. Soc. **19**(13-14), 2551–2562 (1999).
5. A. Licciulli, D. Diso, G. Torsello, S. Tundo, A. Maffezzoli, M. Lomascolo, and M. Mazzer, "The challenge of high-performance selective emitters for thermophotovoltaic applications," Semicond. Sci. Technol. **18**(5), 174–183 (2003).
6. V. M. Marchenko, "Selective visible and near-IR emission of Er_2O_3 excited by a 10.6-µm CO_2 laser," Quantum Electron. **36**(8), 727–730 (2006).
7. J. Llorca and V. M. Orera, "Directionally-solidified eutectic ceramic oxides," Prog. Mater. Sci. **51**(6), 711–809 (2006).
8. D. Sola, F. J. Ester, P. B. Oliete, and J. I. Peña, "Study of the stability of the molten zone and the stresses induced during the growth of Al_2O_3–$Y_3Al_5O_{12}$ eutectic composite by the laser floating zone technique," J. Eur. Ceram. Soc. **31**(7), 1211–1218 (2011).
9. F. J. Ester, D. Sola, and J. I. Peña, "Thermal stresses in the Al_2O_3-$ZrO_2(Y_2O_3)$ eutectic composite during the growth by the laser floating zone technique," Bol. Soc. Esp. Ceram. **47**, 352–357 (2008).
10. J. A. Pardo, J. I. Peña, R. I. Merino, R. Cases, A. Larrea, and V. M. Orera, "Spectroscopic properties of Er^{3+} and Nd^{3+} doped glasses with $0.8CaSiO_3$-$0.2Ca_3(PO_4)_2$ eutectic composition," J. Non-Cryst. Solids **298**(1), 23–31 (2002).
11. D. Sola, R. Balda, J. I. Peña, and J. Fernández, "Site-selective laser spectroscopy of Nd^{3+} ions in $0.8CaSiO_3$-$0.2Ca_3(PO_4)_2$ biocompatible eutectic glass-ceramics," Opt. Express **20**(10), 10701–10711 (2012).
12. D. Sola, R. Balda, M. Al-Saleh, J. I. Peña, and J. Fernández, "Time-resolved fluorescence line-narrowing of Eu^{3+} in biocompatible eutectic glass-ceramics," Opt. Express **21**(5), 6561–6571 (2013).

13. H. Sai, H. Yugami, K. Nakamura, N. Nakagawa, H. Ohtsubo, and S. Maruyama, "Selective emission of $Al_2O_3/E_3Al_5O_{12}$ eutectic composite for thermophotovoltaic generation of electricity," Jpn. J. Appl. Phys. **39**(Part 1, No. 4A), 1957–1961 (2000).
14. N. Nakagawa, H. Ohtsubo, Y. Waku, and H. Yugami, "Thermal emission properties of $Al_2O_3/E_3Al_5O_{12}$ eutectic ceramics," J. Eur. Ceram. Soc. **25**(8), 1285–1291 (2005).
15. M. C. Mesa, P. B. Oliete, R. I. Merino, and V. M. Orera, "Optical absorption and selective thermal emission in directionally solidified Al_2O_3–$Er_3Al_5O_{12}$ and Al_2O_3–$Er_3Al_5O_{12}$–ZrO_2 eutectics," J. Eur. Ceram. Soc. **33**(13-14), 2587–2596 (2013).
16. M. C. Mesa, P. B. Oliete, V. M. Orera, J. Y. Pastor, A. Martín, and J. Llorca, "Microstructure and mechanical properties of $Al_2O_3/Er_3Al_5O_{12}$ eutectic rods grown by the laser-heated floating zone method," J. Eur. Ceram. Soc. **31**(7), 1241–1250 (2011).
17. M. C. Mesa, P. B. Oliete, and A. Larrea, "Microstructural stability at elevated temperatures of directionally solidified $Al_2O_3/Er_3Al_5O_{12}$ eutectic ceramics," J. Cryst. Growth **360**, 119–122 (2012).
18. P. Wu and A. D. Pelton, "Coupled thermodynamic-phase diagram assessment of the rare earth oxide-aluminium oxide binary systems," J. Alloys Compd. **179**(1-2), 259–287 (1992).
19. K. A. Jackson and J. D. Hunt, "Lamellar and rod eutectic growth," Trans. Metall. Soc. AIME **236**, 1129–1142 (1966).
20. J. Y. Pastor, J. LLorca, A. Salazar, P. B. Oliete, I. de Francisco, and J. I. Pena, "Mechanical properties of melt-grown alumina–yttrium aluminum garnet eutectics up to 1900 K," J. Am. Ceram. Soc. **88**(6), 1488–1495 (2005).
21. A. Larrea, V. M. Orera, R. I. Merino, and J. I. Peña, "Microstructure and mechanical properties of Al_2O_3-YSZ and Al_2O_3-YAG directionally solidified eutectic plates," J. Eur. Ceram. Soc. **25**(8), 1419–1429 (2005).
22. V. V. Golovlev, C. H. Winston Chen, and W. R. Garrett, "Heat to light energy conversion by emitters doped with rare-earth metal ions," Appl. Phys. Lett. **69**(2), 280–282 (1996).

1. Introduction

Electromagnetic radiation emitted by hot materials has drawn scientist's attention over the last two centuries. Control, adjustment and optimization of spectral emittance of Selective Emitters (SE), i.e. materials whose thermal-radiation emission at equilibrium occurs in a much narrower spectral region compared with a blackbody at the same temperature, have progressed mainly based on trial and error empirical approaches in the search for the appropriate combination of chemical and microstructural properties [1]. Although practical applications of spectrally tailored thermal sources date back to the 19th century, it is in the early 1960s when the new idea of thermophotovoltaic (TPV) power conversion was conceived. In TPV energy conversion, the Selective Emitter converts thermal energy to near infrared radiation at wavelengths where photovoltaic (PV) energy conversion is efficient [2–4]. A TPV system consists of three main components; a heat source, an emitter and a photovoltaic cell array. The energy of the thermally emitted photons matches the semiconductor bandgap of the TPV cell, thus converting photons above the bandgap energy directly into electricity. The major differences with solar energy conversion are the significantly higher density of radiant energy emitted by the source per unit area (1 kWm^{-2} in solar converters, up to 300 kWm^{-2} in TPV converters), the source temperature (i.e. 5600 °C at the surface of the Sun compared to 1000–1500 °C for a typical TPV radiator) but, most of all, the tunability of the TPV source whose emission can be made to peak just above the band edge of the PV cells and to drop at longer wavelengths to minimize heat loss so that the source can reach higher operating temperatures [5,6].

Materials combining selective emission with thermo-structural properties such as good resistance to thermal shocks or to large temperature cycles are very interesting for a variety of different applications ranging from aerospace to energy conversion. These materials are expected not only to exhibit very tight functional properties but also to operate under extreme conditions, where very high temperatures are generally combined with oxidizing atmosphere and strong thermally-induced stress at the same time. The operating temperatures required by these applications are typically in the range of 1000-2000 °C, where functional and thermo-structural properties are equally important and must therefore be optimized at the same time so that the best balance between functional and thermo-structural requirements must be found. Attention has mainly been focused on refractory systems containing rare earths, but other

ceramic systems have also been investigated [2–6]. In particular, eutectic ceramics are very suitable to operate under these extreme environmental and working conditions.

Eutectic ceramics are composite materials formed in situ from a melt. The development of eutectic ceramic composites has been of great interest because of the fine microstructure control that can be carried out by the solidification conditions [7–9]. The alternation of two or more crystalline phases, joined at atomic level with micrometric spacing, lead to different geometries providing the material properties that depend on the nature of the phases [7]. Directionally solidified eutectic (DSE) ceramic oxides are particularly interesting due to their outstanding mechanical properties, microstructural stability, and corrosion resistance up to temperatures very close to their melting point which make them suitable for functional and structural purposes [7]. Furthermore, they can also be used for optical applications, since eutectics are usually made from large optical band gap materials and present the unusual characteristic of being at the same time a monolith and a multiphase material, and thus, the optically active ions can be placed in different crystal field environments in the same material [10–12].

Selective emission of Er^{3+} in directionally solidified Al_2O_3-$Er_3Al_5O_{12}$ eutectic ceramics has previously been investigated in samples processed by Bridgman and Laser Floating Zone (LFZ) techniques [13–15]. Samples manufactured by means of the LFZ technique showed better thermo-structural properties which make them suitable for high temperature applications such as Selective Emitter in TPV converters [16,17].

In this work we report, for the first time to the best of our knowledge, the fabrication of directionally solidified Al_2O_3-$Er_3Al_5O_{12}$ eutectic ceramic layers in planar geometry. For this purpose we have developed an innovative method based on the manufacturing of these DSE layers departing from Al_2O_3-$Er_3Al_5O_{12}$ eutectic particles of sub-milimetric size. These eutectic particles have also been produced by directional solidification in planar geometry. The originality of this method relies firstly, on the fabrication of sub-milimetric Selective Emitter eutectic particles by this technique, which is innovative in itself. Secondly, departing from eutectic particles allows direct manufacturing of DSE Al_2O_3-$Er_3Al_5O_{12}$ dense crack-free Selective Emitter layers in one go without pre-heating or post-cooling requirements, since the eutectic particles retain the outstanding thermo-mechanical properties provided by the eutectic microstructure. This processing route overcomes the main drawbacks of manufacturing DSE ceramic layers in planar geometry departing from sintered powder. In this way, this novel method provides an easier and direct route for producing TPV devices based on DSE ceramics.

We have characterized microstructural, mechanical and thermal emission properties of eutectic particles and DSE layers in order to assess their features as Selective Emitters.

2. Experimental

Eutectic precursors were obtained from the powder mixture of Al_2O_3 (Aldrich, 99.99%) and Er_2O_3 (Alfa Aesar, 99.99%) in the eutectic composition 81% and 19% mol% respectively [18]. Eutectic mixture was sintered at 1500 °C for 12 hours and processed in planar geometry by using a CO_2 laser (Electronic Engineering, Blade 600) at a mean continuous power of 70 W and solidification rates of 180 and 720 mm/h to obtain two types of eutectic particles, which from now on will be called EP1 and EP2. Afterwards, each one of the eutectic particles were milled in alumina mortar to reduce the size to the sub-milimetric range and next uniaxially pressed at 390 MPa for 1 minute to obtain eutectic pellets. Finally, directionally solidified eutectic layers were obtained by processing the pellets in planar geometry by using laser power of 70 W and processing rates of 180 and 720 mm/h. Figure 1 shows the laser processing sketch. A cylindrical optical lens was used to focus the CO_2 laser radiation in a linear beam. Once the sample surface was placed at focal plane, a 1-axis monitorized positioning system (PI Micos, LS-110) was used to move the sample.

Microstructural and semi-quantitative compositional analyses were determined by Field Emission Scanning Electron Microscopy, FESEM, (Carl Zeiss, MERLIN) with Energy Dispersive X-ray Spectroscopy, EDX, detector incorporated. Mechanical characterization was carried out in terms of nano-hardness and Young modulus by using a nano-indenter (Agilent Technologies, G200). Thermal emission spectra were measured on the directionally solidified eutectic surface and on the departing eutectic particles for comparison purposes by heating the samples with the CO_2 laser unfocused and perpendicular to the sample surface, producing a heated surface of around 5 mm diameter. Emitted light was collected by using a 1000 µm diameter optical fiber. To study the influence of collecting angle, the fiber was positioned at 0, 30 and 60° with regard to the sample surface, where 0° means parallel to the surface. Emission was detected in the 800–2500 nm range using an NIR spectrometer (Ocean Optic, NIR256).
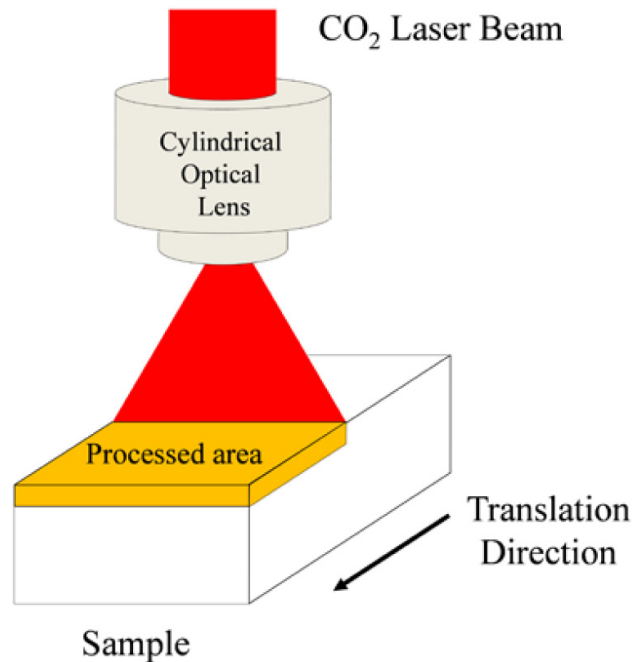

Fig. 1. Laser processing sketch used to manufacture eutectic samples in planar geometry.

3. Results and discussion

3.1 Microstructural and mechanical characterization

In order to analyze the effects appeared in the microstructure as a consequence of eutectic particle nature and solidification rate, a microstructural analysis was carried out by means of SEM and EDX.

Firstly, the eutectic composites obtained after pellets laser processing were analyzed. As an example Fig. 2(a) shows a transverse cross-section view micrograph of a sample processed at 720 mm/h departing from eutectic particles EP1. Laser power used in the process partially melted the pellet producing a directionally solidified layer. Both the directionally solidified layer and the non-molten area can be observed in this Figure. The directionally solidified layer presented a thickness around 160 ± 10 µm. It was found that layer thickness was correlated to the processing rate, increasing at around 210 ± 5 µm in samples solidified at 180 mm/h.

Figure 2(b) presents a detail of the molten layer. A dense, free of cracks and pores layer was obtained. Only two phases (dark and light contrasts) were observed. EDX phase identification determined that black phase corresponded to Al_2O_3 and white phase to $Er_3Al_5O_{12}$. The microstructure consisted of a homogeneous 3D interpenetrated network of both eutectic phases, also referred to as Chinese Script microstructure, in agreement with previous studies reported in cylindrical geometry [16].

Non-molten zone microstructure, shown in Fig. 2(c), presented a great heterogeneity, with areas in which interpenetrated microstructure was found, whereas in other areas one of the two phases predominated. In addition, these areas presented high porosity as a consequence of uniaxial pressing procedure carried out to produce the eutectic pellets.
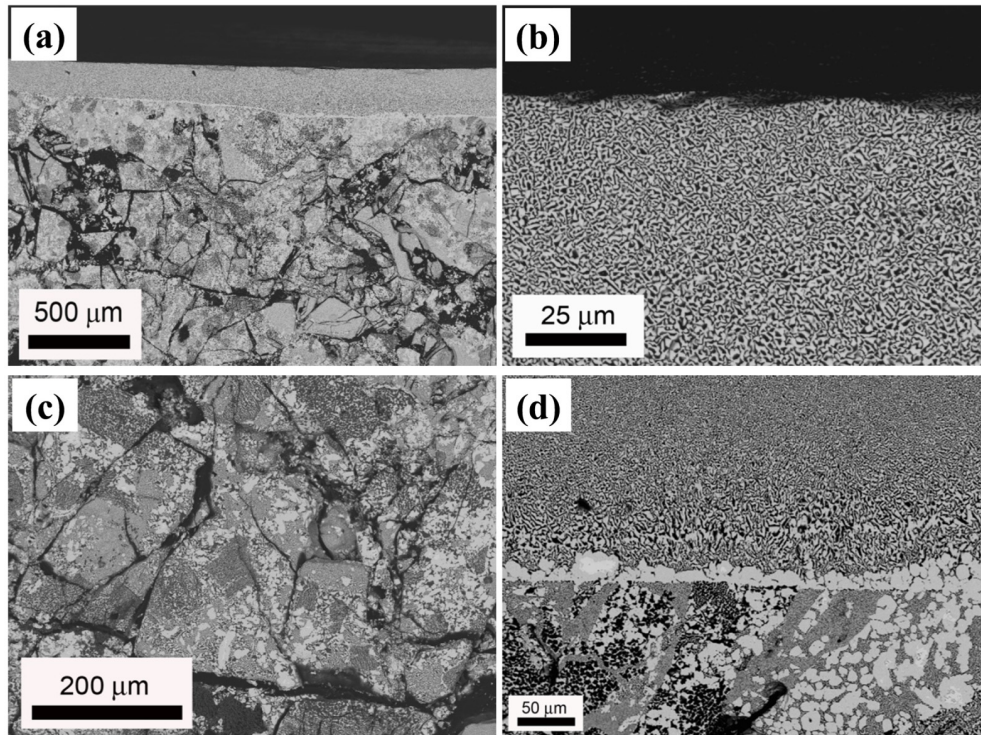

Fig. 2. Transverse cross-section micrograph of sample processed at 720 mm/h from eutectic particles produced at 180 mm/h (a). Details of directionally solidified layer (b), eutectic particles in non-molten zone (c), and interphase between molten layer and eutectic particles (d).

It is worth mentioning that all processed samples showed phase thickening when approaching the interphase between molten layer and eutectic particles. Moreover, $Er_3Al_5O_{12}$ (EAG) phase layer could be produced in the interphase, Fig. 2(d). These phenomena were due to the thermal gradient produced during the laser processing since solidification takes place slower in the inside of the sample than on the sample surface, giving rise to microstructural thickening. These features were general for all processed samples.

Strong dependence of microstructure on solidification rate was found, in accordance with Hunt-Jackson law [19], with phase size refinement and hence decrease of interphase spacing λ with the increase of the processing rate. Figure 3 depicts a detail of the area with eutectic microstructure in particles obtained at 180 mm/h, EP1, and 720 mm/h, EP2, (a) and (b) respectively. It can be observed how the increase in the processing rate gave rise to a thinner microstructure. In particular, interphase spacing λ, defined as the length between two consecutive EAG crystals, and determined by linear analysis of SEM cross-section

micrographs, was found to be 636 ± 100 nm and 276 ± 50 nm for EP1 and EP2 respectively. A similar behavior was observed in the directionally solidified layer so that the higher the processing rate the lower the interphase spacing. As an example, Figs. 4(a) and 4(b) show directionally solidified eutectic layers produced processing at 180 mm/h departing from EP1 and at 720 mm/h departing from EP2 in which interphase spacing was found to be 952 ± 150 nm and 444 ± 100 nm respectively.

Hardness and Young modulus were determined from Vickers nano-indentation tests at room temperature. Recorded values for samples processed at 180 and 720 mm/h departing from EP2 were 17.6 ± 1.1 GPa and 17.7 ± 5.2 GPa respectively for hardness, and 264.9 ± 10.3 GPa and 293.1 ± 37.3 GPa respectively for Young modulus. These values were in the same range than for the obtained in cylindrical geometry [16], and close to the measured in directionally solidified Al_2O_3-$Y_3Al_5O_{12}$ eutectics [20,21].
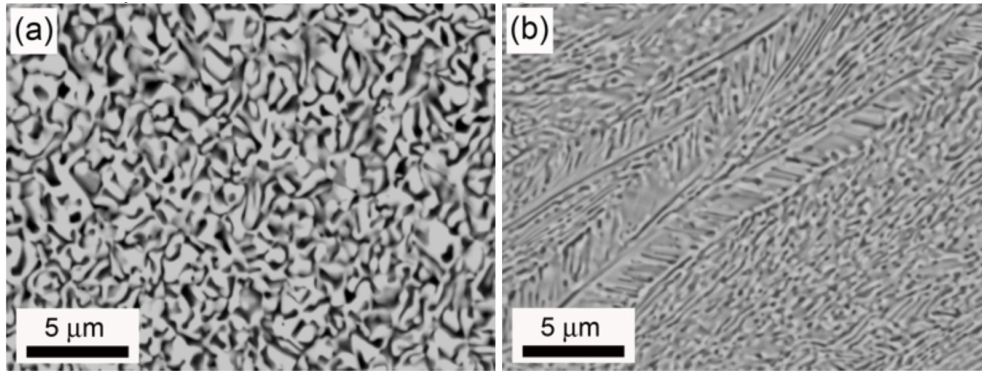

Fig. 3. Transverse micrograph of eutectic microstructure in particles obtained at 180 mm/h, EP1, and 720 mm/h, EP2, (a) and (b) respectively.
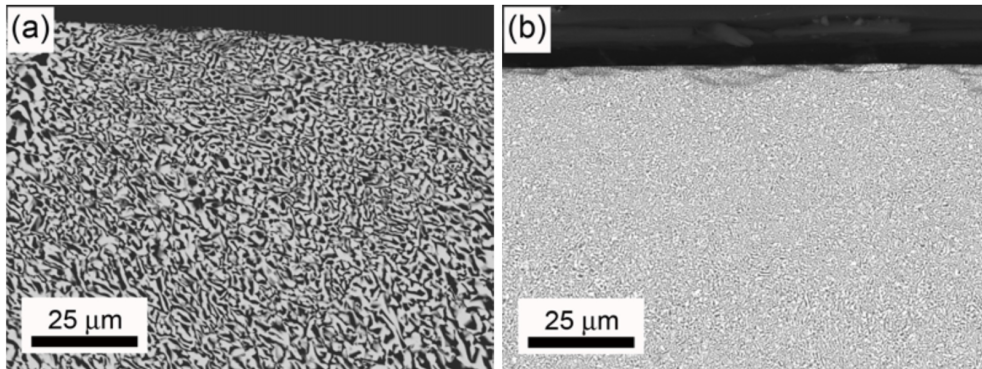

Fig. 4. Transverse micrograph of directionally solidified eutectic layers produced processing at 180 mm/h departing from EP1, (a), and at 720 mm/h departing from EP2, (b).

3.2 Selective thermal emission

Thermal emission of directionally solidified eutectic ceramics obtained in planar geometry were assessed by using a CO_2 laser as a heating source, analyzing the influence of departing eutectic particles and processing rates, and hence evaluating the effect of phase size in function of laser power and collecting angle on Er^{3+} ion thermal emission. For this purpose laser power was set at 46, 56 and 83 W, i.e., low, medium and high thermal excitation, and collecting angles at 0, 30 and 60°, in which 0°-configuration was parallel to the surface of the sample and the incoming laser radiation irradiated the sample at 90°. Figures 5(a) and 5(b) show thermal emission spectra for the eutectic sample processed at 180 mm/h from EP2 at 56

W in function of the collecting angle and the corresponding normalized spectra respectively. Thermal emission spectra showed two narrow emission bands, the most intense centered at 1.5 μm and the other at 1 μm, attributed to the Er^{3+} ion radiative transitions from the thermally excited electronic states to the ground state $^4I_{13/2}\rightarrow{}^4I_{15/2}$ and $^4I_{11/2}\rightarrow{}^4I_{15/2}$ respectively. Thermal excitation of the 4f electron to the excited electronic levels was assumed to occur via the phonon-ion coupling [22]. Both emission bands showed certain structure related to the splitting of the Stark components which are related to the environment of crystalline field of Er^{3+} ion in this eutectic ceramic. In particular, the spectra corresponding to the $^4I_{13/2}\rightarrow{}^4I_{15/2}$ transition showed at least four main bands with the most intense peaks located at 1528 nm and 1562 nm, and the corresponding to the $^4I_{11/2}\rightarrow{}^4I_{15/2}$ showed doublet structure. In spite of thermal emission becoming more intense as collecting angle got closer to incoming radiation angle, normalized spectra showed in Fig. 5(b) revealed that structure of emission bands was independent from collecting angle. Thus, based on this result, collecting angle was fixed at 0° for the following thermal characterization experiments.
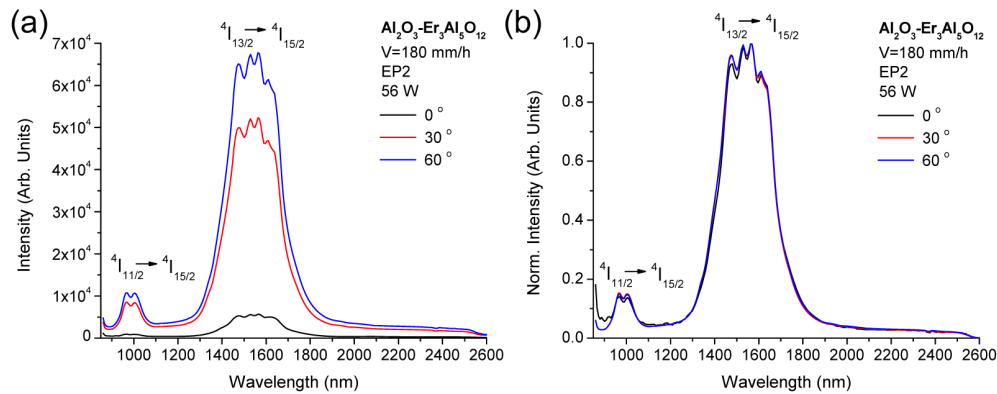

Fig. 5. Thermal emission spectra for the eutectic sample processed at 180 mm/h from EP2 at 56 W in function of the collecting angle, (a), and the corresponding normalized spectra, (b).

Next, thermal emission was studied in function of microstructural features and laser power. Figure 6 shows spectra recorded for the sample processed at 720 mm/h departing from eutectic particles EP2 at 46, 56 and 83 W. It can be observed that laser power increase gave rise to a higher intensity in both $^4I_{11/2}\rightarrow{}^4I_{15/2}$ and $^4I_{13/2}\rightarrow{}^4I_{15/2}$ emission bands which was attributed to the increase of Er^{3+} ion electronic excitation with laser power with the subsequent thermal emission increase. At low laser power the $^4I_{11/2}\rightarrow{}^4I_{15/2}$ emission band at 1 μm was almost negligible but the increase of laser power at medium or high values entailed the development of a doublet structure. In addition, the development of this emission band with laser power increase was related with a shift of the center of gravity of the $^4I_{13/2}\rightarrow{}^4I_{15/2}$ emission band to higher energies, i.e. to lower wavelengths, in accordance to Wien's displacement law. In particular, the relative intensity of the highest and the lowest energy components of this emission band, placed around 1481 nm and 1610 nm, varied so that the appearance of the $^4I_{11/2}\rightarrow{}^4I_{15/2}$ emission band produced an increase in the emission intensity of the highest energy component and a decrease in the lowest energy component. Specifically, designating peak intensities at the shortest and longest wavelengths as I_S and I_L, the ratios I_S/I_L at 46 W and 83 W were 0.908 and 1.045 respectively. This blue shift to lower wavelengths with temperature increase allowed correlating laser power with sample temperature. Taking into account the ratio of the highest intensity values of the 1 μm and 1.5 μm emission bands, $I_{1μm}/I_{1.5μm}$, at 46, 56 and 83 W, and assuming that emissivity in both emission bands did not change [4], sample temperature was calculated relating the resulting ratio values to the blackbody spectra ratio at these wavelengths, obtaining 716, 797, and 947 °C for 46, 56, and

83 W respectively. With regard to the processing rate, the $^4I_{13/2}\rightarrow^4I_{15/2}$ emission band at 1.5 µm was slightly more defined for the sample obtained at the lowest rate, 180 mm/h. Nevertheless, these differences can be considered no significant. These features were common independently of the departing eutectic particles.

Finally, thermal emission spectra of DSE layers were compared to the recorded for eutectic particles EP1 and EP2. As an example, Fig. 7 shows emission spectra of molten layer produced at 180 mm/h departing from EP1, and the corresponding to EP1, both at laser power of 83 W. For comparison purposes, thermal emission spectra of DSE manufactured in cylindrical geometry at 25 mm/h, AE25, is also included [15]. As shown in Fig. 7, eutectic particles thermal emission showed selective emission with similar features to those already described above for directionally solidified molten layers in planar geometry. Furthermore, thermal emission of these samples presented a more selective emission, i.e. emission out of Er^{3+} emission bands was lower than those produced by the Bridgman technique [14]. Worth noting is that thermal emission of both DSE layers and eutectic particles presented significant differences when compared to the obtained in cylindrical geometry. Emission band at 1.5 µm presented more structure and higher number of Stark components. Specifically, low energy peak at 1610 nm did not appear in AE25 sample. Moreover, doublet structure observed in the 1 µm emission band turned into singlet structure in cylindrical geometry samples.

In spite of the differences observed in thermal emission spectra in function of the manufacturing method, the match of 1.5 µm emission bands with InGaAs PV cell photoemission was highly remarkable, as shown in Fig. 7.
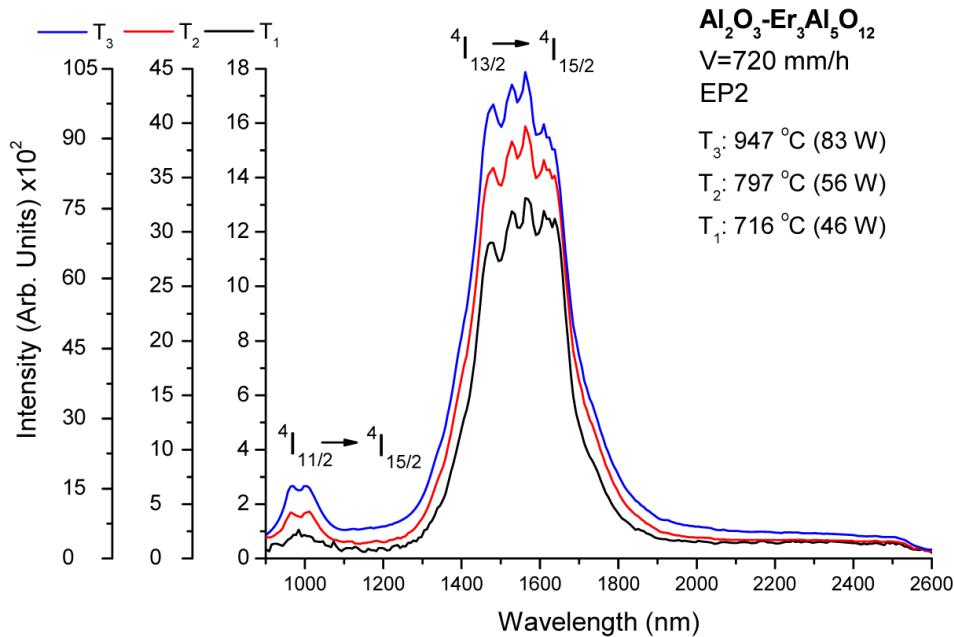

Fig. 6. Thermal emission spectra for samples processed at 720 mm/h departing from eutectic particles EP2 at 716 °C (46 W), 797 °C (56 W) and 947 °C (83 W), (a), (b), and (c) respectively.
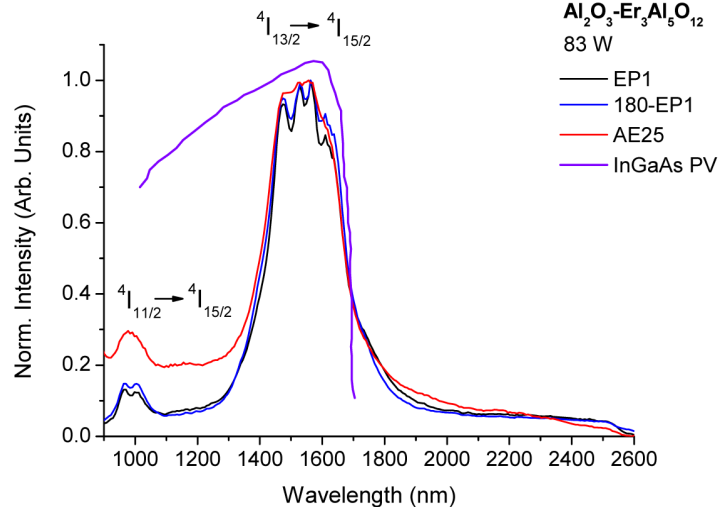
Fig. 7. Thermal emission spectra of eutectic particles EP1, and DSE layers processed at 180 mm/h departing from EP1, both at 83 W. Thermal emission spectra of DSE manufactured in cylindrical geometry at a rate of 25 mm/h, AE25 [15], and InGaAs PV cell photoemission.

4. Conclusions

Directionally solidified Al_2O_3-$Er_3Al_5O_{12}$ eutectic composite was successfully manufactured in planar geometry departing from eutectic particles. Both eutectic particles and molten layers were produced at solidifying rates of 180 and 720 mm/h.

Microstructural analysis determined that samples had homogeneous and interpenetrated microstructure. Strong dependence of microstructure on solidification rate was found. According to Hunt-Jackson law, interphase spacing decreased with processing rate.

Samples presented similar mechanical properties than the reported in previous works produced in cylindrical geometry by means of the Laser Floating Zone technique, with hardness around 17 GPa and Young modulus around 300 GPa.

Directionally solidified eutectic layers in planar geometry and eutectic particles presented selective thermal emission. Thermal emission characterization showed that eutectic samples had two emission bands: one broad and high intensity band at 1.5 µm which matches with InGaAs PV cell, and therefore which could be used for selective emitter applications, and one low intensity band at 1 µm. In particular, $^4I_{13/2} \rightarrow {}^4I_{15/2}$ emission band at 1.5 µm was made up of four main components and $^4I_{11/2} \rightarrow {}^4I_{15/2}$ emission band at 1 µm presented doublet structure. It was found that emission bands structure was independent of the collecting angle. Furthermore, doublet structure development depended on incoming laser power so that this emission band was only presented at medium or high laser power. In addition, it was also found that appearance of doublet structure was correlated to the variation of emission intensity of the highest and lowest energy components of $^4I_{13/2} \rightarrow {}^4I_{15/2}$ emission band. Spectral features were nearly independent of departing eutectic particles and showed small differences with regard to the processing rate.

These results open up the possibility of manufacturing TPV devices based on directionally solidified Al_2O_3-$Er_3Al_5O_{12}$ eutectic layers in planar geometry closer to final application as well as the fabrication of sub-milimetric eutectic selective emitter particles.

Acknowledgments